Applied Energy 237 (2019) 682–694

Contents lists available at ScienceDirect

Applied Energy

journal homepage: www.elsevier.com/locate/apenergy

The improved open-circuit voltage characterization test using active polarization voltage reduction method

Jufeng Yang[a,b], Wenxin Huang[a], Bing Xia[b,c], Chris Mi[b,*]

[a] Department of Electrical Engineering, Nanjing University of Aeronautics and Astronautics, 29 Jiangjun Street, Nanjing, Jiangsu 211106, China
[b] Department of Electrical and Computer Engineering, San Diego State University, 5500 Campanile Drive, San Diego, CA 92182, USA
[c] Department of Electrical and Computer Engineering, University of California San Diego, 9500 Gilman Dr., La Jolla, CA 92093, USA

HIGHLIGHTS

- Applied an extra current excitation to reduce polarization voltage.
- Analyzed parametric sensitivity of current excitation to model parameters.
- Developed a method to determine the parameters for the current excitation.
- Shortened the test time due to the active polarization voltage reduction.
- Validated the feasibility and superiority with experiments.

ARTICLE INFO

Keywords:
Lithium-ion battery
Open-circuit voltage (OCV)
OCV characterization test
Equivalent circuit model (ECM)
Polarization effect
Relaxation behavior

ABSTRACT

The correlation between state of charge (SoC) and open-circuit voltage (OCV) is a crucial characteristic parameter in many aspects of the battery management system (BMS). However, it is a challenging task to obtain the accurate SoC-OCV correlation with a high test efficiency. In this paper, an improved OCV characterization test is proposed to actively reduce the polarization voltage. Based on the third-order equivalent circuit model (ECM), two sets of current pulses are applied to accelerate the convergence of the battery terminal voltage, thus the test time is effectively shortened compared to the conventional incremental OCV characterization test. Furthermore, the parametric sensitivity of the imposed current excitation to battery model parameters is analyzed. Subsequently, the parametric determination method for the imposed current excitation is provided. Experiments are conducted on a lithium-ion polymer battery to prove the feasibility of the proposed test procedure. Comparison with the conventional OCV characterization test further demonstrated the superiority of the proposed test procedure.

1. Introduction

In recent years, lithium-ion batteries have become the favorable choice for electric vehicles (EVs) due to their low self-discharge rate, long cycle life, high energy and power capabilities [1,2]. Nevertheless, despite the above advantages, a well-designed battery management system (BMS) is still crucial to ensure the safe and reliable operation of the battery system. Several essential states of batteries, including the state of charge (SoC) [3], state of power (SoP) [4], and state of health (SoH) [5,6] should be monitored accurately by the BMS. In advanced monitoring algorithms, the accurate estimation of battery states is generally associated with the correlation between SoC and open-circuit voltage (OCV). In the SoC estimation technique, the commonly used coulomb counting-based estimation method is often combined with the OCV-based estimation method to determine the initial SoC and recalibrate the estimation result [7,8]. For the SoP estimation, the SoC-OCV correlation is also an important characteristic parameter to calculate the peak current [9]. In addition, the SoC-OCV curve can be employed to identify the battery aging level through differential voltage analysis or incremental capacity analysis techniques [10,11]. Hence, the OCV as a function of SoC is a critical characteristic parameter in many aspects of the battery technology.

1.1. Review of the literature

When the battery is under the current excitation, the measured

* Corresponding author.
E-mail addresses: nuaayjf@163.com (J. Yang), huangwx@nuaa.edu.cn (W. Huang), bixia@eng.ucsd.edu (B. Xia), cmi@sdsu.edu (C. Mi).

https://doi.org/10.1016/j.apenergy.2019.01.060
Received 13 May 2018; Received in revised form 1 January 2019; Accepted 7 January 2019
Available online 14 January 2019
0306-2619/

terminal voltage involves not only the OCV but also the overvoltage representing a series of polarization effects. Since these effects cannot be measured directly by physical sensors and can exist up to several hours after the current interruption, the battery terminal voltage only approximates the OCV after the long-time relaxation process, until all polarization effects nearly vanish [12]. Hence, it is a challenging task to obtain OCV values over a wide SoC range with high accuracy and efficiency. Generally, there are two typical kinds of methods to determine the SoC-OCV correlation: model-based and test-based methods.

The model-based methods generally estimate the polarization voltage V_p based on the equivalent circuit model (ECM), then the battery OCV can be calculated by subtracting V_p from the measured terminal voltage. This type of methods can be further classified into two groups, namely, the OCV prediction methods in the idle condition and the OCV estimation methods in the operation condition. The former group of methods generally utilize the voltage relaxation model to asymptotically fit the measured battery terminal voltage after the current interruption, then the OCV can be predicted by extrapolating the employed voltage relaxation model. In [13] the battery OCV is predicted by an adaptive approach, and the employed model consists of a ZARC-element and a voltage source in series. Ref. [14] establishes an asymptotic function to approximate the battery relaxation behavior, and the extrapolation of the voltage relaxation allows a fast prediction of the battery OCV. From the perspective of the OCV estimation methods in the operation condition, the battery OCV along with other battery parameters (e.g., SoC, impedance parameters, and capacity) are usually identified based on the estimation difference between the model output voltage and the measured terminal voltage. A variety of filters or observers, such as recursive least squares [15], extended Kalman filter [16], H-infinity filter [17], adaptive observer [18], etc., are employed to recursively minimize the estimation difference. One common advantage of the model-based methods is that the long-time relaxation process is not needed to eliminate the influence of the polarization voltage, as the battery OCV can be obtained online. However, it has to be noted that three disadvantages exist concerning this type of technique. Firstly, the accuracy of the obtained OCV is closely related to the fidelity of the employed model. However, because of the limited computational capability of the onboard microcontroller, the employed model is not guaranteed to characterize the polarization effects as precisely as possible [19]. As a result, the estimated OCV generally deviates from the actual value as it consists of the overvoltages representing slow-dynamics polarization effects (e.g., the effect of diffusion processes etc.). Secondly, the complete SoC-OCV correlation is only available when the battery experiences the full discharge/charge process. In fact, only pieces of the SoC-OCV correlation can be obtained due to the incomplete real conditions (especially driving cycles in EVs). In order to obtain a complete SoC-OCV correlation, Ref. [20] proposes a data pieces-based parameter identification method to connect multiple SoC-OCV pieces. However, it requires a large amount of test data pieces to cover a wide SoC range. Thirdly, the OCV and other model parameters are integrated together in the estimation process, thus the cross interference caused by the integration can lead to an inaccurate OCV estimation, which is especially pronounced for the OCV estimation methods in the operation condition [15,21].

For the test-based methods, the polarization voltage is generally reduced or even eliminated during the test procedure, thus the OCV can be obtained directly from the battery terminal voltage. One of the commonly used test-based methods is the low-current OCV characterization test, which employs the low C-rate (e.g. C/20) constant-current (CC) to discharge/charge the battery [8,22–24]. The advantage of this method is that the resolution of the SoC-OCV correlation is high, because of the continuous SoC variation during the test. However, even with the low C-rate, the polarization effects still exist because of the continuous current excitation, especially at extreme SoC ranges, which affects the accuracy of the obtained OCV [25]. An alternative test-based method is the incremental OCV characterization test. In which the battery is discharged/charged incrementally (e.g. 10% SoC interval), and followed by a long-time relaxation process [26–30]. Refs. [14,17,24] have concluded that the SoC-OCV correlation obtained from the incremental OCV characterization test is more reliable than from the low-current OCV characterization test. It is mainly because in the incremental OCV characterization test, polarization effects are nearly eliminated after the long-time relaxation process. Thus, the directly measured terminal voltage can be considered as the battery OCV. However, due to the long-time relaxation process, an extensive test time is required to obtain the complete SoC-OCV correlation for the incremental OCV characterization test.

1.2. Contributions of the paper

Based on the aforementioned analysis, the test-based methods, especially the incremental OCV characterization test, can obtain the SoC-OCV correlation with a higher accuracy, in comparison to model-based methods. However, the long relaxation time makes the whole test too time-consuming. As the long-time relaxation process is used to eliminate the influence of the polarization voltage, we had a question, why not we actively minimize the polarization voltage to accelerate the convergence speed of the battery terminal voltage? Hence, an improved OCV characterization test using active polarization voltage reduction method is proposed in this paper. The main contributions of this paper are:

(1) A certain form of the current excitation is first introduced to accelerate the voltage convergence of the RC network. By analyzing the overvoltage across the first-order RC network, it is proved that the voltage response under the specific current excitation shows a faster convergence performance, in comparison to that under the self-rest condition.
(2) Two sets of current pulses are applied to ensure a fast convergence of the battery terminal voltage. According to the frequency range of physical processes occurring under the open-circuit condition, a third-order ECM is adopted to describe the relaxation behavior. Based on the employed ECM, two sets of current pulses are utilized to actively minimize the overvoltages across the middle- and long-term RC networks, which correspond to the effects of middle- and low-frequency polarizations, respectively.
(3) The parameter calculation method is provided to predetermine the imposed current excitation. The impact of the model parameter variation on the imposed current parameters is investigated. Based on this, the parameter calculation method considering the influence of the SoC is provided. The experiment results demonstrate the superiority of the proposed test method in terms of the convergence speed.

2. Battery relaxation model

The ECM is widely employed to characterize the physical processes occurring in the battery [31–33]. The common structure of an ECM is shown in Fig. 1, where the ideal voltage source V_{OC} stands for the OCV, the Ohmic resistance R_o is related to the electrolyte and connection

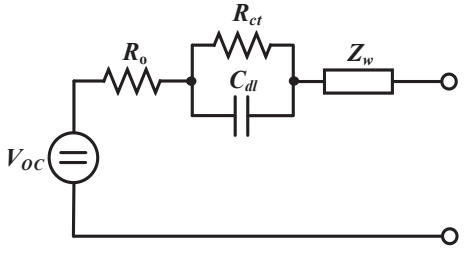

Fig. 1. The general equivalent circuit model.

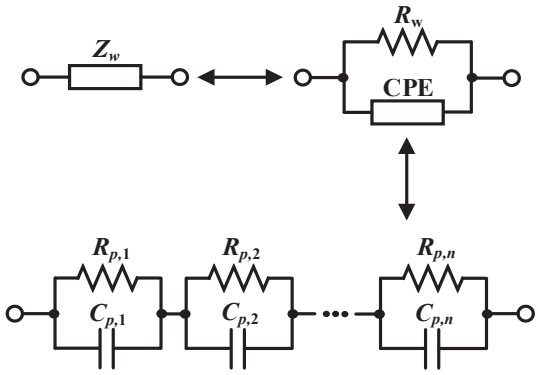

Fig. 2. The equivalent circuit models to represent the concentration polarization processes.

resistance, the RC network ($R_{p,ct}//C_{p,dl}$) represents the effect of the activation polarization (charge-transfer and double-layer), and the Warburg impedance Z_w is correlated with the effect of the concentration polarization (mass transport), which is mainly due to the diffusion processes.

In general, the majority of the concentration polarization processes have larger time constants compared to the Ohmic resistance and activation polarization processes [34]. Hence, the concentration polarization is largely responsible for the overvoltage variation during the long-term relaxation process. Typically, considering a limited-length diffusion condition and neglecting the high-frequency dynamics, the Warburg impedance Z_w can be represented by a parallel resistance R_w and constant phase element (CPE) circuit as illustrated in Fig. 2, and the corresponding impedance is expressed as [13,35]

$$Z_{R_w//Z_{CPE}} = \frac{R_w}{1 + R_w \cdot A_0 \cdot (j\cdot\omega)^{\alpha}} \tag{1}$$

where A_0 is a parameter of CPE, α is the depression parameter. By applying an inverse transformation on (1) to the time domain, it can be found that the $R_w//Z_{CPE}$ circuit can be completely modeled by an infinite number of RC networks with slightly different time constants, as shown in Fig. 2 [36].

The ECM shown in Fig. 2 consists of a large number of circuit parameters, which would result in the massive parameterization effort and the convergence problem [4,37]. Generally, the frequency domain of the concentration polarization covers a wide range of frequency, from 10^{-5} Hz up to 10^{0} Hz [38]. It is a good compromise to abandon the extremely low-frequency component because the corresponding overvoltage built up during the incremental charge/discharge period is negligible. Besides, compared to completely modeling of polarization effects, the RC networks which represent typical dynamic characteristics of polarization effects would be needed for the proposed method as will be discussed in Section 3. Hence, considering the tradeoff among the parameterization effort, the convergence performance and the model fidelity, a third-order RC network with different orders of time constants is employed to characterize the effect of the concentration polarization in this study. Specifically, effects of activation and high-frequency concentration polarizations are modeled as one RC network ($R_{p,1}//C_{p,1}$) due to similar frequency characteristics.

The detailed architecture of the ECM with the third-order RC network is shown in Fig. 3 [39,40], where $V_{p,i}$ (i = 1, 2, 3) denotes the overvoltage across the corresponding RC network ($R_{p,i}//C_{p,i}$). Specifically, the time constant of $R_{p,i}//C_{p,i}$ increases with the increasing index, i.e., $V_{p,1}$, $V_{p,2}$ and $V_{p,3}$ model the overvoltages caused by the high-, middle- and low- frequency polarization effects, respectively, as illustrated in Fig. 3.

The electrical behavior of the third-order ECM can be expressed as

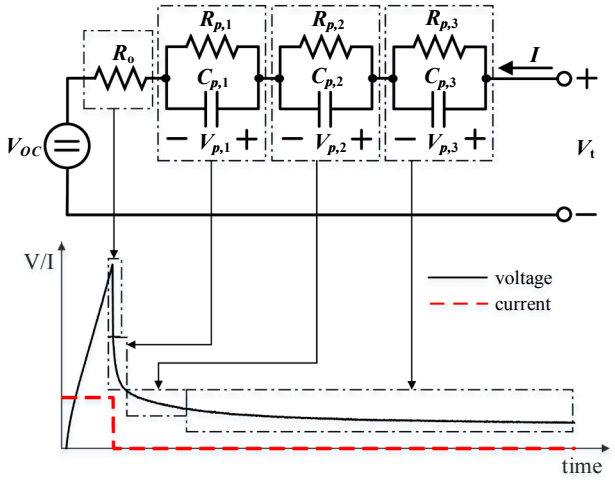

Fig. 3. The third-order equivalent circuit model.

$$C_{p,i}\frac{dV_{p,i}}{dt} + \frac{V_{p,i}}{R_{p,i}} = I \tag{2}$$

$$V_t = V_{OC} + IR_o + \sum_{i=1}^{3} V_{p,i} \tag{3}$$

where $R_{p,i}$ and $C_{p,i}$ represent the polarization resistance and the polarization capacitance, respectively, V_t represents the battery terminal voltage, and I is the load current (the positive value denotes charging and the negative value denotes discharging).

Specifically, the detailed expression of $V_{p,i}$ can be derived by solving (2),

$$V_{p,i}(t) = V_{p,i}(0)\exp(-t/\tau_{p,i}) + IR_{p,i}[1 - \exp(-t/\tau_{p,i})] \tag{4}$$

where $V_{p,i}(0)$ represents the initial overvoltage across the corresponding RC network, which is caused by the preceding charge or discharge period, $\tau_{p,i}$ (i = 1, 2, 3) is the time constant of the corresponding RC network and $\tau_{p,i} = R_{p,i}\cdot C_{p,i}$.

It should be noted that the load current I equals zero under the open-circuit condition, thus the overvoltage across R_o can be omitted. Hence, the overvoltage caused by the polarization effects during the relaxation period can be expressed as

$$V_{p,i}(t) = V_t(t) - V_{OC}(t) = \sum_{i=1}^{3} V_{p,i}(0)\exp(-t/\tau_{p,i}) \tag{5}$$

3. Proposed active polarization voltage reduction method

As mentioned above, the overvoltages caused by the middle- and low-frequency polarization effects can be modeled as $V_{p,2}$ and $V_{p,3}$ in the third-order ECM, and a long period of relaxation time is generally required for them to reach the steady state. However, based on the characteristic of the RC network, a certain form of the current excitation can be applied to accelerate the voltage convergence, which will be illustrated in detail as follows.

3.1. Analysis of the RC network voltage response

3.1.1. The first-order RC network

Considering a scenario that the RC network is firstly discharged by a current pulse with amplitude $|I_p|$ and time duration T_p, the corresponding voltage response at time T_p (point B in Fig. 4(a)) can be derived based on (4),

$$V_{p,curr}(T_p) = V_p(0)\exp(-T_p/\tau_p) - |I_p|\ R_p[1 - \exp(-T_p/\tau_p)] \tag{6}$$

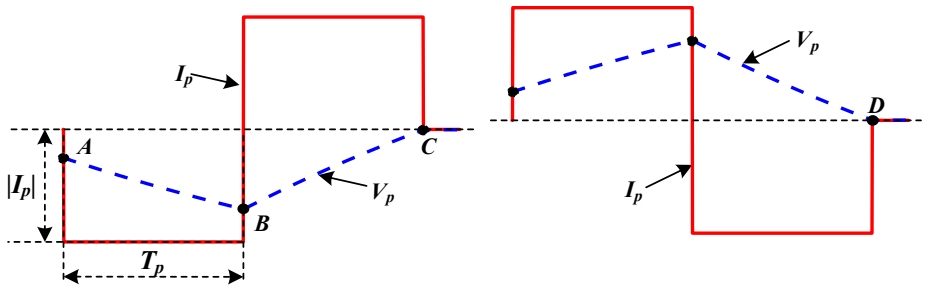

(a) Scenario 1. (b) Scenario 2.

Fig. 4. Schematic of current excitations (solid line) and corresponding voltage responses (dashed line).

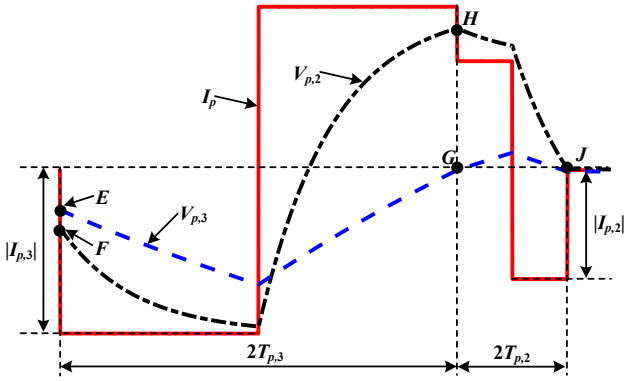

Fig. 5. Schematic of the proposed current excitation (solid line) and corresponding voltage responses (dashed lines).

where I_p represents the imposed current, a positive value represents the charging case and a negative value represents the discharging case, $V_p(0)$ is the overvoltage across the RC network at the beginning of the current pulse (point A in Fig. 4(a)), which can be expressed as

$$V_p(0) = I_d R_p[1 - \exp(-T_d/\tau_p)] \tag{7}$$

where I_d and T_d are the current and the time duration of the preceding charge/discharge period, respectively.

Afterwards, the RC network is immediately charged by a current pulse with the same amplitude and time duration, as shown in Fig. 4(a). The corresponding voltage response at the end of the second current pulse (point C in Fig. 4(a)) can be expressed as

$$V_{p,curr}(2T_p) = V_{p,curr}(T_p)\exp(-T_p/\tau_p) + |I_p|\, R_p[1 - \exp(-T_p/\tau_p)] \tag{8}$$

Substituting (6) into (8), $V_{p,curr}(2T_p)$ can be further expressed as

$$V_{p,curr}(2T_p) = V_p(0)\exp(-2T_p/\tau_p) + |I_p|\, R_p[1 - \exp(-T_p/\tau_p)]^2 \tag{9}$$

For the self-rest scenario, the RC network voltage at time $2T_p$ is expressed as

$$V_{p,rest}(2T_p) = V_p(0)\exp(-2T_p/\tau_p) \tag{10}$$

It can be concluded from (9) and (10) that $V_{p,curr}(2T_p)$ is larger than $V_{p,rest}(2T_p)$ because of the second term in (9). In other words, if $V_p(0)$ is negative, $V_{p,curr}$ will converge toward zero first in comparison to $V_{p,rest}$.

Similarly, if the RC network is imposed by the current excitation as shown in Fig. 4(b) (scenario 2), the corresponding voltage response at point D is expressed as

$$V_{p,curr}(2T_p) = V_p(0)\exp(-2T_p/\tau_p) - |I_p|\, R_p[1 - \exp(-T_p/\tau_p)]^2 \tag{11}$$

It can be concluded from (10) and (11) that $V_{p,curr}$ after this kind of current excitation is lower than $V_{p,rest}$ after the relaxation time of $2T_p$, which means that $V_{p,curr}$ also shows a faster convergence speed with the positive initial value compared to $V_{p,rest}$.

3.1.2. The second-order RC network

Based on the aforementioned analysis, the RC network voltage shows a faster convergence speed under the specific set of current pulses. In addition, since the charge and discharge pulses possess the same current amplitude and duration, the values of SoC before and after the current excitation are identical. Hence, in the incremental OCV characterization test, the predesigned current excitation can be employed to actively reduce the polarization voltage, and thus the test time is shortened. For the fast-dynamics polarization effects, a short period of relaxation time is required for the corresponding overvoltage $V_{p,1}$ to reach the steady state. Hence, in this study, only the polarization voltages represented by $V_{p,2}$ and $V_{p,3}$ are actively reduced due to the slow dynamic characteristics. To simplify the discussion, only the incremental discharge test is considered in this study. The derivation for the charge case can be conducted in a similar way.

Since $V_{p,3}$ caused by the low-frequency polarization effects is the main factor to the long relaxation time, a set of current pulses (the waveform is similar to that in Fig. 4(a)) are first imposed on the battery to accelerate the convergence of $V_{p,3}$. Assuming $V_{p,3}$ equals zero at the end of the current excitation (point G in Fig. 5), the relevant current amplitude $|I_{p,3}|$ and the time duration $T_{p,3}$ should be constrained by the following equation

$$V_{p,3}(2T_{p,3}) = V_{p,3}(0)\exp(-2T_{p,3}/\tau_{p,3}) + |I_{p,3}|\, R_{p,3}[1 - \exp(-T_{p,3}/\tau_{p,3})]^2 = 0 \tag{12}$$

where $V_{p,3}(0)$ is negative after the preceding discharge period (point E in Fig. 5).

For the middle-term RC network ($R_{p,2}//C_{p,2}$), the corresponding overvoltage at time $2T_{p,3}$ can be expressed as

$$V_{p,2}(2T_{p,3}) = V_{p,2}(0)\exp(-2T_{p,3}/\tau_{p,2}) + |I_{p,3}|\, R_{p,2}[1 - \exp(-T_{p,3}/\tau_{p,2})]^2 \tag{13}$$

Considering the values of T_d and $T_{p,3}$, (referring to Section 4), and the change rate of the exponential function (referring to Appendix A), it can be obtained that

$$\exp(-T_d/\tau_{p,i}) \approx \exp(-T_{p,3}/\tau_{p,i}) \tag{14}$$

Hence, (12) can be further rewritten as follows on the basis of (7) and (14).

$$-1 = \frac{V_{p,3}(0)\exp(-2T_{p,3}/\tau_{p,3})}{|I_{p,3}|\, R_{p,3}[1 - \exp(-T_{p,3}/\tau_{p,3})]^2} = \frac{I_d \exp(-2T_{p,3}/\tau_{p,3})}{|I_{p,3}|[1 - \exp(-T_{p,3}/\tau_{p,3})]} \tag{15}$$

Since $\tau_{p,2}$ and $\tau_{p,3}$ are well-separated (time constants can be considered as well-separated if $\tau_{p,3} \geq 5\tau_{p,2}$ [41]), it can be derived that

$$\exp(-2T_{p,3}/\tau_{p,2}) < \exp(-2T_{p,3}/\tau_{p,3}) \tag{16}$$

$$1 - \exp(-T_{p,3}/\tau_{p,2}) > 1 - \exp(-T_{p,3}/\tau_{p,3}) \tag{17}$$

Based on (15), (16) and (17), the following relationship can be

obtained.

$$-1 = \frac{V_{p,3}(0)\exp(-2T_{p,3}/\tau_{p,3})}{|I_{p,3}|\ R_{p,3}[1-\exp(-T_{p,3}/\tau_{p,3})]^2} < \frac{V_{p,2}(0)\exp(-2T_{p,3}/\tau_{p,2})}{|I_{p,3}|\ R_{p,2}[1-\exp(-T_{p,3}/\tau_{p,2})]^2} < 0 \tag{18}$$

Considering (13) and (18), it can be further obtained that

$$V_{p,2}(2T_{p,3}) = V_{p,2}(0)\exp(-2T_{p,3}/\tau_{p,2}) + |I_{p,3}|\ R_{p,2}[1-\exp(-T_{p,3}/\tau_{p,2})]^2 > 0 \tag{19}$$

It concludes that $V_{p,2}(2T_{p,3})$ can be qualitatively determined as the positive value, as shown in Fig. 5 (point H). Hence, the polarization voltage represented by $V_{p,2}$ cannot be eliminated or effectively reduced by the above current excitation, and another set of current pulses, with the waveform similar to that in Fig. 4(b), are applied immediately after the first current excitation to overcome the above problem, as shown in Fig. 5. Assuming $V_{p,2}$ equals zero at the end of the current pulses, the following relationship can be derived on the basis of (11).

$$V_{p,2}(2T_{p,2}+2T_{p,3}) = V_{p,2}(2T_{p,3})\exp(-2T_{p,2}/\tau_{p,2}) - |I_{p,2}|\ R_{p,2}[1-\exp(-T_{p,2}/\tau_{p,2})]^2 = 0 \tag{20}$$

Theoretically, $V_{p,2}$ can be eliminated after the second set of current pulses. On the other hand, since $V_{p,3}(2T_{p,3}) = 0$, $V_{p,3}$ at time $2T_{p,3} + 2T_{p,2}$ (point J in Fig. 5) can be expressed as

$$V_{p,3}(2T_{p,3}+2T_{p,2}) = -|I_{p,2}|\ R_{p,3}[1-\exp(-T_{p,2}/\tau_{p,3})]^2 \tag{21}$$

Generally, $T_{p,2}$ is far less than $\tau_{p,3}$, which can be verified from the designed parameters in Section 4. Hence, the term $[1-\exp(-T_{p,2}/\tau_{p,3})]^2$ in (21) is close to zero and $V_{p,3}$ maintains a low value after the second set of current pulses.

3.2. Parameter determination of the imposed current excitation

3.2.1. Relationship between $|I_{p,i}|$ and $T_{p,i}$

Based on (12) and (20), $|I_{p,i}|$ can be obtained with the predetermined $T_{p,i}$.

$$|I_{p,i}| = \frac{|V_{p,i,init}|\ \exp(-2T_{p,i}/\tau_{p,i})}{R_{p,i}[1-\exp(-T_{p,i}/\tau_{p,i})]^2}, \qquad i = 2,\ 3 \tag{22}$$

where $|V_{p,i,init}|$ is the amplitude of the initial RC network voltage at the beginning of relevant current pulses, such as point E ($i = 3$) and point H ($i = 2$) in Fig. 5. For the long-term RC network ($i = 3$), $|V_{p,3,init}|$ is defined as

$$|V_{p,3,init}| = |I_d|\ R_{p,3,d}[1-\exp(-T_d/\tau_{p,3})] \tag{23}$$

where $R_{p,3,d}$ is the average long-term resistance covering the incremental discharge period.

For the middle-term RC network ($i = 2$), $|V_{p,2,init}|$ is defined as

$$\begin{cases} |V_{p,2,init}| = |V_{p,2}(T_d)|\exp(-2T_{p,3}/\tau_{p,2}) + |I_{p,3}|\ R_{p,2}[1-\exp(-T_{p,3}/\tau_{p,2})]^2 \\ |V_{p,2}(T_d)| = |I_d|\ R_{p,2,d}[1-\exp(-T_d/\tau_{p,2})] \end{cases} \tag{24}$$

where $R_{p,2,d}$ is the average middle-term resistance covering the incremental discharge period, $V_{p,2}(T_d)$ is the overvoltage caused by the incremental discharge period (point F in Fig. 5).

It can be concluded from (22)–(24) that except the definition of the initial voltage, the expressions of $|I_{p,i}|$ for two sets of current pulses have the identical form. In order to simplify the analysis, only the relationship between $|I_{p,3}|$ and $T_{p,3}$ is discussed in this section.

Based on (22) and (23), the evolution of $|I_{p,3}|$ (in the form of C-rate) with respect to $T_{p,3}$ is plotted as a solid curve in Fig. 6. In addition, the dashed curve in Fig. 6 illustrates the SoC variation during one charge/discharge pulse (ΔSoC_3) with respect to the different $T_{p,3}$. The parameters in (22) and (23), i.e., $|I_d|$, T_d, $R_{p,3,d}$, $R_{p,3}$ and $\tau_{p,3}$, are obtained from the impedance characterization test at around 30% SoC. It can be seen from the figure that both $|I_{p,3}|$ and ΔSoC_3 achieve high values with the low $T_{p,3}$. For example, when $T_{p,3}$ is selected as 6 min, the corresponding $|I_{p,3}|$ and ΔSoC_3 are 4.614C and 46.14%, respectively (i.e., point K in Fig. 6). For most of the lithium-ion batteries, such a long duration and high C-rate load current are harmful. Moreover, the battery terminal voltage will reach the cutoff value easily because of the large values of $|I_{p,3}|$ and ΔSoC_3 [42]. Besides, due to the variation of battery model parameters, $|I_{p,3}|$ and $T_{p,3}$ with respect to the large ΔSoC_3 will differ greatly from the value shown in Fig. 6, which will be further discussed in Sections 3.2.2 and 5.1. For this reason, $V_{p,3}$ may not be effectively reduced under the current excitation with respect to the large ΔSoC_3. On the other hand, it can be observed from Fig. 6 that both $|I_{p,3}|$ and ΔSoC_3 decrease exponentially with the increase of $T_{p,3}$, which means that a larger $T_{p,3}$ can overcome above problems. However, a larger $T_{p,3}$ results in a longer test time. Hence, a compromise between the test time and $|I_{p,3}|$ (or ΔSoC_3) must be considered when determining the appropriate parameters of the current excitation.

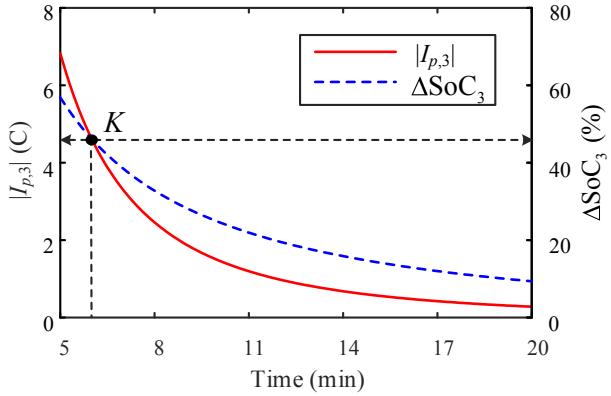

Fig. 6. Evolution of $|I_{p,3}|$ and ΔSoC_3 with respect to $T_{p,3}$.

3.2.2. Sensitivity of $|I_{p,3}|$ to battery model parameters

It can be concluded from (22) that besides $T_{p,3}$ and $V_{p,3,init}$, battery model parameters, i.e., $R_{p,3}$ and $\tau_{p,3}$, also have a great influence on the determination of $|I_{p,3}|$. Hence, the sensitivity of $|I_{p,3}|$ to battery model parameters is worth investigating.

Considering the variations of battery model parameters, Eq. (22) can be rewritten as

$$|\widetilde{I}_{p,3}| = \frac{|V_{p,3,init}|\ \exp(-2T_{p,3}/\widetilde{\tau}_{p,3})}{\widetilde{R}_{p,3}[1-\exp(-T_{p,3}/\widetilde{\tau}_{p,3})]^2} \tag{25}$$

where $|\widetilde{I}_{p,3}|$ is the amplitude of the current pulse when parameter variations exist, $\widetilde{R}_{p,3}$and$\widetilde{\tau}_{p,3}$are battery model parameters considering variation values, which can be expressed as

$$\begin{cases} \widetilde{R}_{p,3} = R_{p,3} + \Delta R_{p,3} \\ \widetilde{\tau}_{p,3} = \tau_{p,3} + \Delta\tau_{p,3} \end{cases} \tag{26}$$

where $\Delta R_{p,3}$ and $\Delta\tau_{p,3}$ are variation values on model parameters.

By subtracting (22) and (25), $\Delta\ |I_{p,3}| = |I_{p,3}| - |\widetilde{I}_{p,3}|$ is obtained to quantitatively evaluate the variation of $|I_{p,3}|$ caused by the model parameter variation. Similar to the previous analysis, the assumed model parameters are extracted from the impedance characterization test data at 30% SoC, and $T_{p,3}$ is predetermined as 10 min. Simulation results are shown in Fig. 7. It can be summarized that: (1) $|I_{p,3}|$ is more sensitive to the parameter variation on $\tau_{p,3}$ when the corresponding variation rate is above −40%. (2) The impact of the model parameter variation is not negligible. The $|I_{p,3}|$ change can reach up to 1.49C and 2.181C with −50% variation rate on $R_{p,3}$ and 50% variation rate on $\tau_{p,3}$, respectively. Hence, the sensitivity study gives us an important guide for the parametric determination of the imposed current pulses.

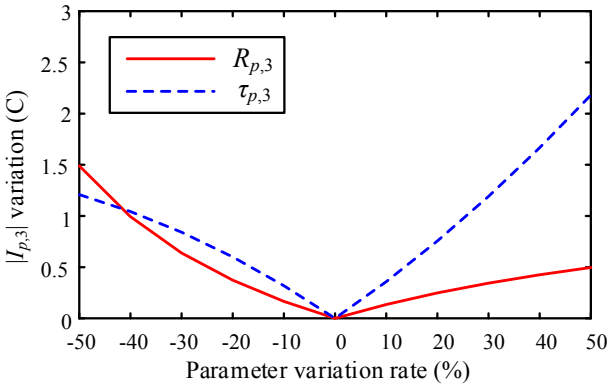

Fig. 7. Sensitivity of $|I_{p,3}|$ to the variation of battery model parameters.

3.2.3. Determination of $|I_{p,i}|$ and $T_{p,i}$

As indicated in the sensitivity analysis, the stability of battery model parameters, especially $\tau_{p,i}$, during the imposed current pulse is vital to determine current excitation parameters. Since battery model parameters can be considered as functions of SoC, ΔSoC_i should be constrained to a certain range to reduce the model parameter variation. Hence, $|I_{p,i}|$ and $T_{p,i}$ can be determined by the following two constrained equations

$$\begin{cases} |V_{p,i,init}| \exp(-2T_{p,i}/\bar{\tau}_{p,i}) - |I_{p,i}| \bar{R}_{p,i}[1 - \exp(-T_{p,i}/\bar{\tau}_{p,i})]^2 = 0 \\ |I_{p,i}| \ T_{p,i}/(3600C_{cap}) = \Delta SoC_i \end{cases} \quad i = 2, \quad 3 \tag{27}$$

where C_{cap} is the capacity of the battery in Ah, $\bar{R}_{p,i}$ and $\bar{\tau}_{p,i}$ are average values of relevant battery model parameters covering the SoC variation period (ΔSoC_i). Besides, ΔSoC_i should be determined based on the battery impedance identification results. The above equations can be solved by the MATLAB fsolve function.

4. Experimental validation

4.1. Experimental setup

A test platform as shown in Fig. 8 is established to validate the proposed OCV characterization test. A lithium-ion polymer pouch-type battery with 20 A h nominal capacity (model C020 manufactured by EIG) is adopted in this study. The cathode material is Li[NiCoMn]O_2–based and the anode material is graphite-based. Detailed specifications of the tested battery are listed in Table 1. An Arbin BT2000 cycle-based tester and a host computer are used to conduct the test

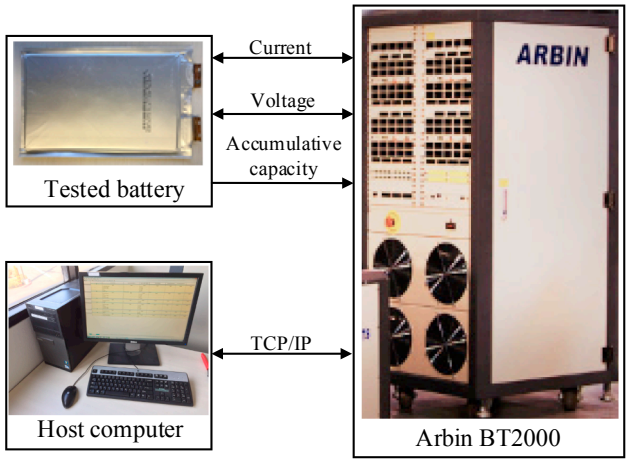

Fig. 8. Configuration of the experimental setup.

Table 1
Specifications of the tested battery.

Type	Li[NiCoMn]O_2
Nominal capacity	20 Ah
Nominal voltage	3.65 V
Maximum charge voltage	4.15 V
Recommended voltage limit for discharge	3.0 V
Maximum discharge current (continuous)	Up to 5 C current
Maximum discharge current (peak < 10 s)	10 C current

procedure and record the test data. Voltage and current measurement ranges of the battery cycler are 0–5 V and ± 100 A, respectively. All of the tests are conducted at room temperature (25 ± 2 °C), and the measured data sets, including current, voltage and accumulative capacity, are collected with the sampling rate of 1 Hz.

4.2. Impedance characterization test

It can be inferred from the aforementioned analysis that battery model parameters, especially the RC network parameters (i.e., $R_{p,2}$, $R_{p,3}$, $\tau_{p,2}$ and $\tau_{p,3}$), are needed in advance to determine $|I_{p,i}|$ and $T_{p,i}$ (i = 2, 3). In this paper, the battery impedance parameters are identified through the hybrid pulse power characterization (HPPC) test.

4.2.1. Test procedure

In the HPPC test, the battery is first completely charged/discharged at 0.5C rate with the constant-current constant-voltage (CCCV) charge/CC discharge procedure, followed by a 2 h rest. After that, the battery is incrementally discharged/charged in 10% of the nominal capacity with 0.5C rate to the next SoC level, and followed by a certain length of the relaxation period. To stimulate the battery dynamically, one pair of discharge and charge current pulses, each lasting for 10 s and with the amplitude of 2C, is imposed before each incremental discharge/charge period. The above test cycle is repeated until the discharge/charge cutoff voltage is reached.

Generally, the RC network parameters can be identified through the battery terminal voltage measured from the relaxation period. Based on the previous research work, the identified parameters, especially the time constants, are closely related to the length of the relaxation period [34,43]. Besides, the relaxation behaviors at extreme SoC ranges, i.e., the low SoC range for the discharge scenario and the high SoC range for the charge scenario, show a slower dynamic characteristic, compared to those in the middle SoC range [12,27]. Hence, the relaxation time at extreme SoC ranges is selected as 120 min and others are selected as 90 min, as a trade-off between the testing effort and the accuracy of model parameters.

4.2.2. Analysis of test results

The evolution of the relaxation process and the energy efficiency at different SoCs are plotted in Fig. 9.

Fig. 9(a) shows the polarization voltage curves over the relaxation period ($V_{p,I=0}$) at different SoCs, where the solid and dashed lines represent the experimental results from charge and discharge tests, respectively. The polarization voltage is obtained by subtracting the battery terminal voltage at the end of the relaxation period ($V_{t,end}$) from the battery terminal voltage during the relaxation period ($V_{t,I=0}$), i.e., $V_{p,I=0} = V_{t,I=0} - V_{t,end}$. It can be observed from Fig. 9(a) that the battery's polarization voltage does not reach the steady state immediately, and the slow-dynamics part dominates the majority of the relaxation period. Moreover, the SoC affects the relaxation behavior of the battery in terms of the shape and convergence performance. This phenomenon is more obvious at 60% and 70% SoCs for the charge test.

Furthermore, the energy efficiency η_e, which is defined as (28), is adopted to quantitatively relate the measured data with the polarization effects [44,45].

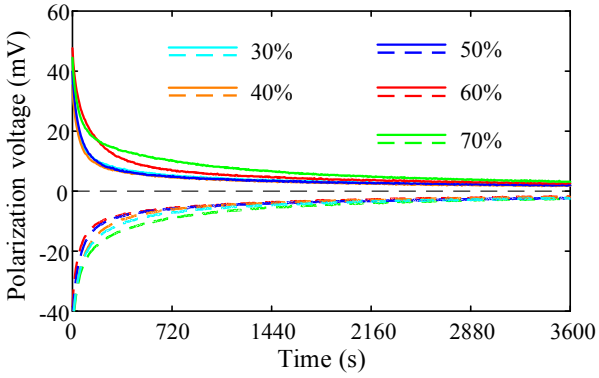

(a) Polarization voltages after charging and discharging at different SoCs under open-circuit condition.

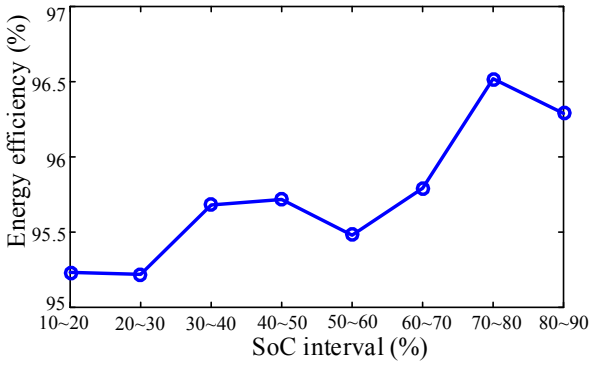

(b) Energy efficiencies during charging and discharging at different SoC intervals.

Fig. 9. Impact of SoC on polarization effects of the battery.

$$\eta_e = E_{dis}/E_{cha} \tag{28}$$

where E_{dis} and E_{cha} represent the discharged energy and the charged energy, respectively. The definitions of E_{dis} and E_{cha} are expressed as

$$\begin{cases} E_{dis} = \int_{I<0} V_t(t)\cdot I(t)dt = \int_{I<0} [V_{OC}(t) + Z_{im}\cdot I(t)]\cdot I(t)dt \\ E_{cha} = \int_{I>0} V_t(t)\cdot I(t)dt = \int_{I>0} [V_{OC}(t) + Z_{im}\cdot I(t)]\cdot I(t)dt \end{cases} \tag{29}$$

where Z_{im} is the impedance representing the Ohmic resistance and the polarization effects, $\int_{I<0}$ and $\int_{I>0}$ are the time integrals over the incremental discharge and charge periods in the impedance characterization test. It can be inferred from (28) and (29) that Z_{im} is mainly responsible for η_e when $I(t)$ is kept constant during the time integral.

The evolution of the energy efficiency is shown in Fig. 9(b). It can be observed that the efficiency generally reduces with decreasing SoC. This variation is mainly contributed to the change in the polarization loss, which is closely related to the battery impedance including Ohmic resistances and polarization effects [45–47]. Hence, it can be preliminarily concluded that the battery impedance is significantly influenced by the SoC.

Based on the curve fitting method presented in Ref. [43], the identified impedance parameters are plotted in Fig. 10. It can be concluded that

(1) Three time constants are well-separated. Specifically, values of the short-, middle- and long-term are in the order of 10 s, 10^2 s and 10^3 s, respectively. Hence, polarization effects occurring in the vicinity of the relevant time constant can be eliminated or reduced by current pulses separately.
(2) The identified impedance parameters vary over a wide SoC range, which is in agreement with the test results shown in Fig. 9. This confirms the necessity of considering the model parameter variation when determining $|I_{p,i}|$ and $T_{p,i}$ (i = 2, 3).
(3) Parameters of the long-term RC network show larger values at extreme SoC ranges, i.e., below 30% SoC for the discharge scenario and above 80% SoC for the charge scenario, compared to values in the other SoC range.

4.3. Comparison of OCV characterization tests

It can be inferred from (27) that besides the RC network parameters, ΔSoC_i should also be determined in advance. Based on the analysis in Section 3.2, the value of ΔSoC_3 is selected around 10% at extreme SoC ranges, and selected around 20% for the other SoC range. For the second set of current pulses, the value of ΔSoC_2 is selected no more than 5%. Hence, the parameters of the imposed current excitation are obtained as illustrated in Fig. 11.

To verify the advantages of the proposed OCV characterization test method, the conventional one is also performed for the purpose of comparison. The current profiles of the conventional and the proposed OCV characterization tests during each SoC interval are schematically shown in Fig. 12. In this paper, the conventional incremental OCV characterization test is conducted with a 4 h relaxation period to allow the battery to approximate the equilibrium. For ease of comparison, a relaxation period of 3.5 h is also employed after the current excitation in the proposed method.

The comparison results between the conventional and the proposed OCV characterization tests at different SoCs are demonstrated in Fig. 13. Specifically, Fig. 13(a)–(c) and (d)–(f) shows the battery's polarization voltage curves over the relaxation period from discharge and charge OCV characterization tests, respectively. It can be observed from Fig. 13 that by the conventional method, the polarization voltage shows the slow convergence performance, and the gradient of the polarization voltage over time is relatively low during the majority of the relaxation period (approximate 2 mV over the last 2.5 h). Moreover, even after the long period of relaxation time, i.e., 4 h in this paper, the polarization voltage still cannot reach the equilibrium state totally. This phenomenon is specifically obvious at 20% SoC of the discharge scenario and 80% SoC of the charge scenario, which is in agreement with the identified time constants demonstrated in Section 4.2. Therefore, it can be concluded that the battery terminal voltage at the end of the relaxation period is still an approximation of the OCV.

By comparison, the polarization voltage obtained from the proposed method converges to the steady state rapidly after the imposed current excitation. Some transient overshoots occur when the current excitation is finished, such as black circle regions in Fig. 13(a), (c) and (d). However, the overshoot dies out shortly and the polarization voltage converges to the steady state as time evolves. The overshoot phenomenon is mostly due to the imposed current excitation. As analyzed beforehand in Section 3.1.2, the imposed current excitation can only eliminate or reduce overvoltages across the middle- and long-term RC networks, which characterize the diffusion processes occurring in middle- and low-frequency regions. For the short-term RC network representing the fast-dynamics polarization effects, the corresponding overvoltage would be discharged/charged away from the steady state under the current excitation. Thus, an extra short-term relaxation period (e.g., 10 min) is required to allow the fast-dynamics polarization effects to finish.

Additionally, it has to be noted that at 20% SoC of the discharge scenario, the polarization voltage still shows a slightly increasing tendency after the current excitation, as shown in Fig. 13(c). It is because the relaxation behavior in the low SoC range shows the slow-dynamics characteristic [12], while RC networks (i.e., $R_{p,2}//C_{p,2}$ and $R_{p,3}//C_{p,3}$) identified from the HPPC test cannot accurately describe relevant electrochemical reactions due to the limited data points, and only the polarization voltage around specific frequency ranges (correspond to

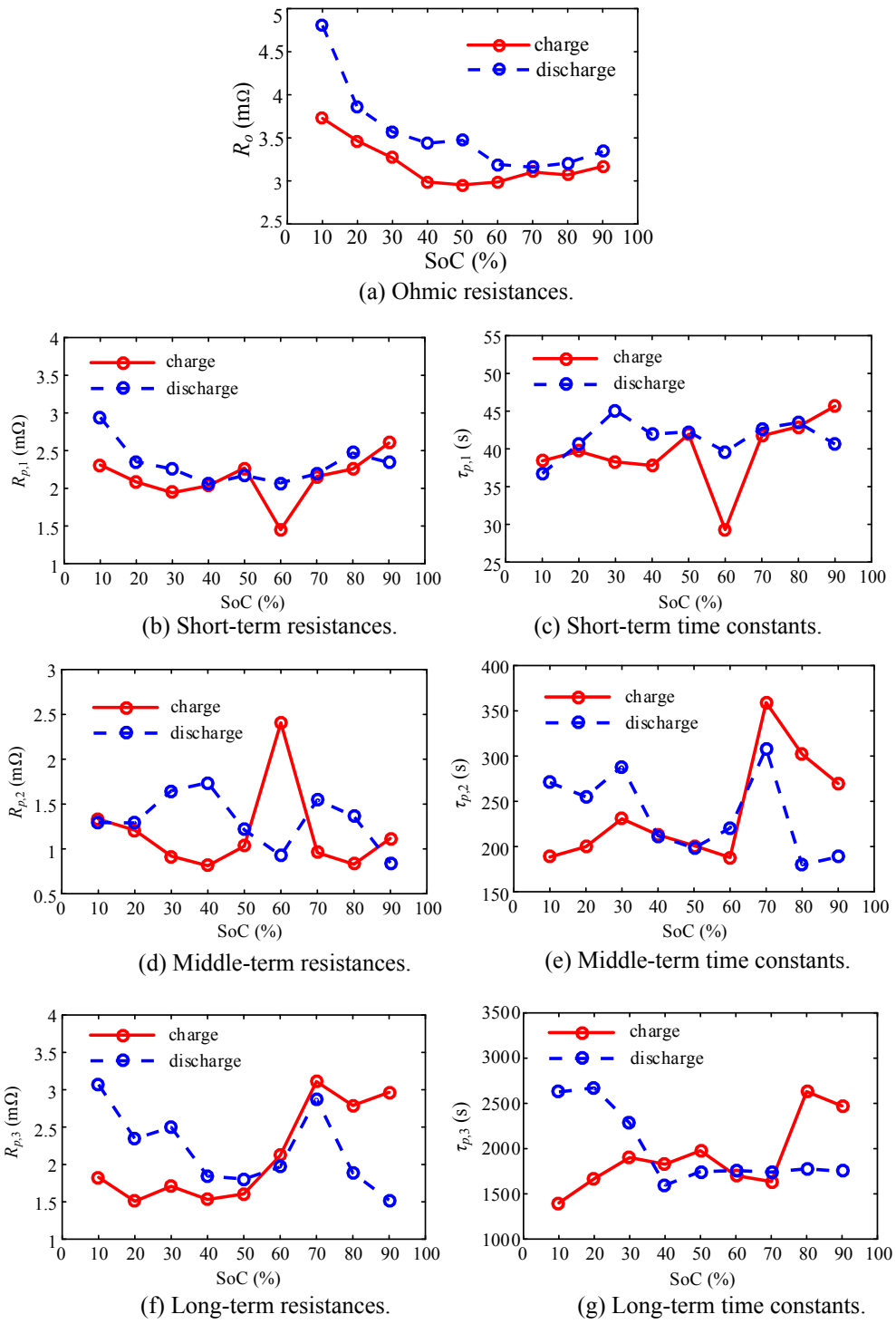

Fig. 10. Identification results of RC network parameters.

identified time constants) can be reduced by the imposed current excitation. However, it can be observed from Fig. 13(c) that the gradient of the polarization voltage over time is considerably small (i.e., 1 mV over 2.5 h), and thus the remaining polarization effect is negligible.

In summary, the proposed method can ensure a fast convergence of the polarization voltage caused by the incremental discharge/charge period, especially with middle- and low-frequency dynamics. In addition, since the long-time relaxation process is unnecessary, the proposed method proves to be more time-saving in comparison to the conventional one.

5. Discussion

5.1. Benefit of considering the model parameter variation

It can be learnt from the HPPC test results that the identified model

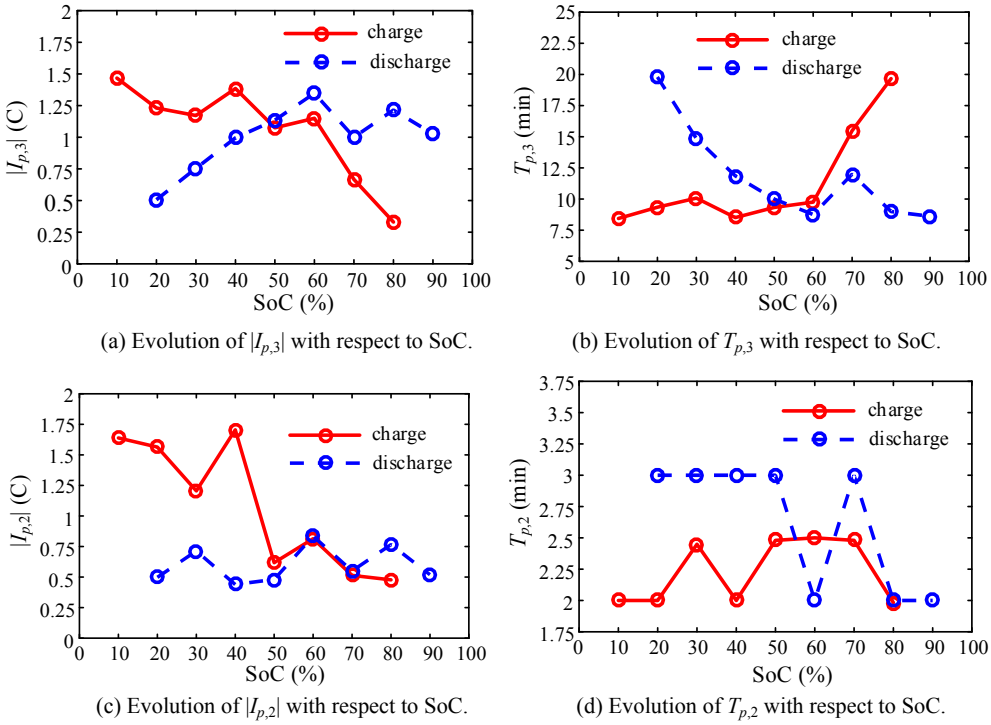

(a) Evolution of $|I_{p,3}|$ with respect to SoC.

(b) Evolution of $T_{p,3}$ with respect to SoC.

(c) Evolution of $|I_{p,2}|$ with respect to SoC.

(d) Evolution of $T_{p,2}$ with respect to SoC.

Fig. 11. Calculated parameters of the imposed current excitation.

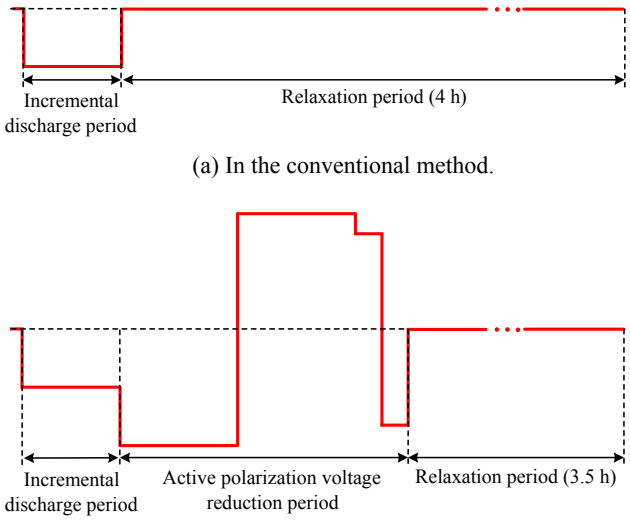

(a) In the conventional method.

(b) In the proposed method.

Fig. 12. Schematic representation of the current profiles of OCV characterization tests during each SoC interval.

parameters change over a wide SoC range, such as the time constant in a SoC range below 30% for the discharge scenario, as demonstrated in Fig. 10. Based on the analysis beforehand in Section 3.2.2, the impact of the model parameter variation on the parametric determination of the current excitation is not negligible. Fig. 14 shows the comparison result of the polarization voltage curves obtained from the conventional and proposed methods, where proposed method #1 and #2 represent the method with and without considering the model parameter variation, respectively. It can be observed from Fig. 14 that for the proposed method #2, although the obtained polarization voltage is generally higher than the value obtained from the conventional method, there still exists the pronounced increasing tendency during the relaxation period. By contrast, the polarization voltage obtained from the proposed method #1 is closer to the steady state. Moreover, the gradient of the polarization voltage over time also decreases to low enough (i.e., 1 mV over 2.5 h) to be neglected.

5.2. OCV measurements at extreme SoC ranges

Taking the discharge OCV characterization test as an example, due to the slow-dynamics relaxation behavior in the low SoC range, large values of $|I_{p,3}|$ or $T_{p,3}$ are generally required to ensure a fast convergence of the polarization voltage. On the one hand, the large $T_{p,3}$ will result in the long test time and reduce the advantage of the proposed method. On the other hand, the large $|I_{p,3}|$ can make the battery terminal voltage reach the cutoff value easily, which in turn leads to the incomplete SoC-OCV correlation [42]. Similarly, for the charge OCV characterization test in the high SoC range, the battery will be charged in the CV mode by the imposed charge current pulse. This will cause the SoC variation at the end of the current excitation to be nonzero, and the shifted SoC-OCV correlation will be obtained eventually. Hence, the conventional long-time relaxation process is employed to measure the OCV at extreme SoC ranges, i.e., below 20% SoC for the discharge scenario and above 80% SoC for the charge scenario in this paper.

5.3. Future work

Generally, the battery aging state and the temperature significantly affect the battery relaxation behavior. In this paper, the tested battery is in a new state and all of the characterization tests are conducted at room temperature (25 ± 2 °C). In order to further verify the feasibility of the proposed method, the performance of the proposed OCV characterization method at different battery aging states and temperatures will be investigated comprehensively in our future work.

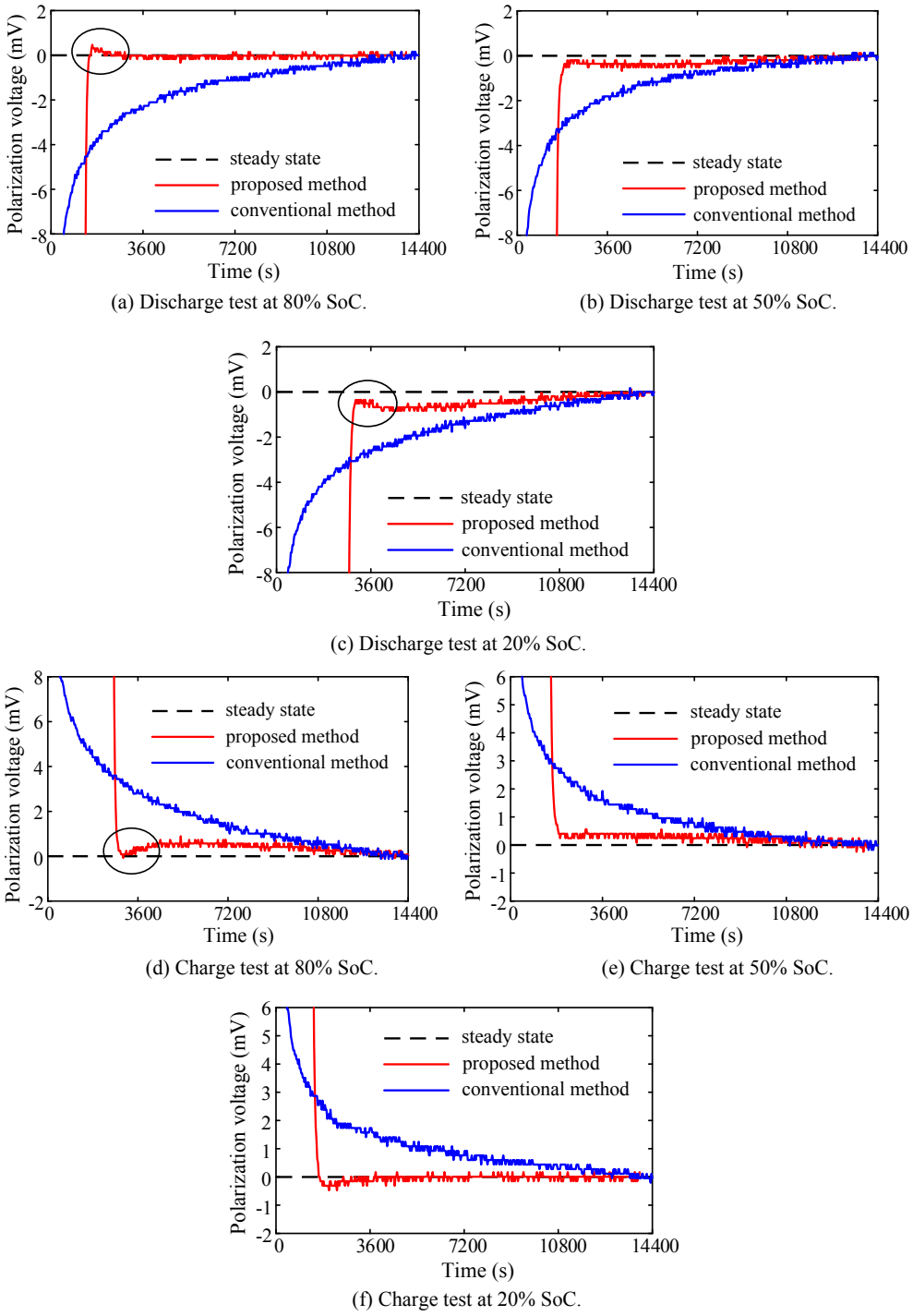

Fig. 13. Evolution of polarization voltage curves after discharge/charge at different SoCs during relaxation period.

6. Conclusion

An improved incremental OCV characterization test is proposed in this paper. Compared with the conventional incremental OCV characterization test, the extra current excitation is imposed immediately after the incremental discharge/charge period, and thus the fast convergence of the battery terminal voltage is achieved. Firstly, the battery's relaxation behavior is broadly divided into three regions (i.e., fast-, middle- and long-frequency regions) according to the order of the magnitude of relevant time constants, and the third-order ECM is employed to describe this behavior. Secondly, based on the characteristic of the RC network, two sets of current pulses are proposed to actively minimize overvoltages across the long- and middle-term RC networks, which correspond to the polarization effects dominating the majority of the relaxation period. Furthermore, the parametric sensitivity of the imposed current excitation to battery model parameters is analyzed, and the parametric determination method for the imposed current excitation is provided subsequently. A lithium-ion polymer battery is

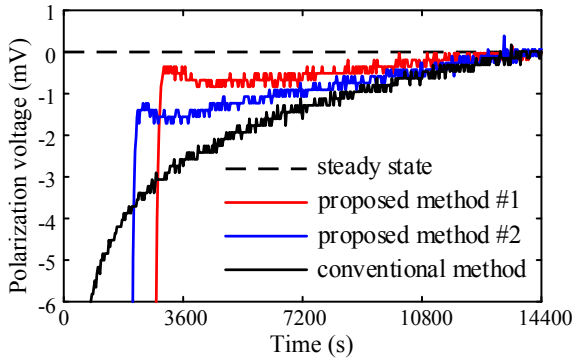

Fig. 14. Comparison of polarization voltage curves obtained after discharge at 20% SoC during relaxation period.

adopted under test to validate the proposed test procedure. Experimental results proved the feasibility of the proposed test procedure, and demonstrated advantages over the conventional one. At last, the benefit of considering the battery model parameter variation and the OCV measurements at extreme SoC ranges are further illustrated in the later discussion.

Acknowledgments

The authors would like to acknowledge the funding support from the China Scholarship Council (CSC); the US DOE Graduate Automotive Technology Education (GATE) Center of Excellence; the National Science Foundation (1507198); and Nanjing Golden Dragon Bus Co., Ltd.

Appendix A

For the exponential function expressed as

$$y = \exp(-x/a) \tag{A.1}$$

where a is a constant, x is the input variable, and y is the output variable. The differentiation of (A.1) in respect to x is expressed as.

$$dy/dx = -\exp(-x/a)/a \tag{A.2}$$

Based on (A.2), Fig. A1 is plotted to illustrate the relationship between x and dy/dx.

It can be concluded from (A.2) and Fig. A1 that the value of dy/dx increases with the increasing x , and the change rate of y approaches zero when x is greater than zero.

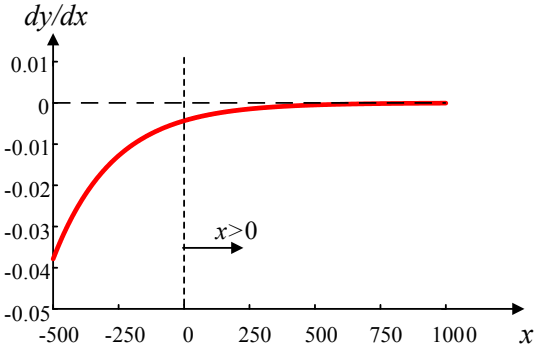

Fig. A1. Relationship between x and dy/dx (exemplarily with a = 230.7, which equals $\tau_{p,2}$ at around 30% SoC).

Appendix B

BMS	battery management system
CC	constant-current
CCCV	constant-current constant-voltage
CPE	constant phase element
ECM	equivalent circuit model
EV	electric vehicle
HPPC	hybrid pulse power characterization
OCV	open-circuit voltage
SoC	state of charge
SoH	state of health
SoP	state of power
A_0	parameter of CPE
C_{cap}	capacity of the battery in Ah
E_{cha}	charged energy
E_{dis}	discharged energy
I	load current
$\|I_d\|$	amplitude of the current during the incremental discharge period
$\|I_p\|$	amplitude of the imposed current pulse
$\|I_{p,3}\|$, $\|I_{p,2}\|$	amplitude of the first and the second set of current pulses
$\|\widetilde{I}_{p,3}\|$	amplitude of the imposed current pulse considering battery model parameter variations

$C_{p,1}$, $C_{p,2}$, $C_{p,3}$	capacitances of three RC networks that model the polarization effects
R_w	resistance of the circuit that represents the Warburg impedance
$R_{p,2,d}$, $R_{p,3,d}$	average middle- and long-term resistance covering the incremental discharge period
$R_{p,1}$, $R_{p,2}$, $R_{p,3}$	resistances of three RC networks that model the polarization effects
$\bar{R}_{p,i}$	average value of $R_{p,i}$ covering the SoC variation period
$\widetilde{R}_{p,3}$	resistance of $R_{p,3}//C_{p,3}$ considering the variation value
$R_{p,ct}//C_{p,dl}$	RC network represents the effect of the activation polarization
R_o	Ohmic resistance
T_d	time duration of the incremental discharge period
T_p	time duration of one current pulse
$2T_{p,3}$, $2T_{p,2}$	time duration of the first and the second set of current pulses
V_{OC}	ideal voltage source stands for the OCV
$V_p(0)$	overvoltage across the RC network at the beginning of the first current pulse
$V_{p,1}$, $V_{p,2}$, $V_{p,3}$	overvoltages of three RC networks that model the polarization effects
$V_{p,1}(0)$, $V_{p,2}(0)$, $V_{p,3}(0)$	initial overvoltages of three RC networks that model the polarization effects
$V_{p,curr}$	voltage response of the RC network under the current excitation
$V_{p,I=0}$	polarization voltage during the relaxation period
$V_{p,i,init}$	RC network voltage at the beginning of relevant current pulses
$V_{p,rest}$	voltage response of the RC network under the self-rest condition
V_t	battery terminal voltage
$V_{t,end}$	battery terminal voltage at the end of the relaxation period
$V_{t,I=0}$	battery terminal voltage during the relaxation period
Z_{im}	impedance representing the Ohmic resistance and polarization effects
Z_w	Warburg impedance
α	depression parameter of CPE
$\tau_{p,1}$, $\tau_{p,2}$, $\tau_{p,3}$	time constants of three RC networks that model the polarization effects
$\bar{\tau}_{p,i}$	average value of $\tau_{p,i}$ covering the SoC variation period
$\widetilde{\tau}_{p,3}$	time constant of $R_{p,3}//C_{p,3}$ considering the variation value
η_e	energy efficiency
$\Delta\lvert I_{p,3}\rvert$	variation of $\lvert I_{p,3}\rvert$ caused by the battery model parameter variation
ΔSoC_2, ΔSoC_3	SoC variation during one charge/discharge pulse
$\Delta\tau_{p,3}$, $\Delta R_{p,3}$	variation values of $\tau_{p,3}$ and $R_{p,3}$

References

[1] Mi C, Masrur MA, Gao DW. Hybrid electric vehicles: principles and applications with practical perspectives; 2011.

[2] Lu L, Han X, Li J, Hua J, Ouyang M. A review on the key issues for lithium-ion battery management in electric vehicles pp. 272–288, 2013/03/15 J Power Sources 2013;226:/.

[3] Yang J, Xia B, Shang Y, Huang W, Mi CC. Adaptive state-of-charge estimation based on a split battery model for electric vehicle applications. IEEE Trans Veh Technol 2017;66:10889–98.

[4] Farmann A, Sauer DU. Comparative study of reduced order equivalent circuit models for on-board state-of-available-power prediction of lithium-ion batteries in electric vehicles 2018/09/01/ Appl Energy 2018;225:1102–22.

[5] Li S, Pischinger S, He C, Liang L, Stapelbroek M. A comparative study of model-based capacity estimation algorithms in dual estimation frameworks for lithium-ion batteries under an accelerated aging test. Appl Energy 2018/02/15/ 2018.;212:1522–36.

[6] Yang J, Xia B, Huang W, Fu Y, Mi C. Online state-of-health estimation for lithium-ion batteries using constant-voltage charging current analysis. Appl Energy 2018/02/15/ 2018.;212:1589–600.

[7] Ng KS, Moo C-S, Chen Y-P, Hsieh Y-C. Enhanced coulomb counting method for estimating state-of-charge and state-of-health of lithium-ion batteries. Appl Energy 2009/09/01/ 2009.;86:1506–11.

[8] Xing Y, He W, Pecht M, Tsui KL. State of charge estimation of lithium-ion batteries using the open-circuit voltage at various ambient temperatures. Appl Energy 2014/01/01/ 2014.;113:106–15.

[9] Sun F, Xiong R, He H, Li W, Aussems JEE. Model-based dynamic multi-parameter method for peak power estimation of lithium–ion batteries. Appl Energy 2012;96:378–86. 2012/08/01/.

[10] Liu G, Ouyang M, Lu L, Li J, Han X. Online estimation of lithium-ion battery remaining discharge capacity through differential voltage analysis. J Power Sources 2015;274:971–89. 2015/01/15/.

[11] Gong X, Xiong R, Mi CC. A data-driven bias-correction-method-based lithium-ion battery modeling approach for electric vehicle applications. IEEE Trans Ind Appl 2016;52:1759–65.

[12] Farmann A, Sauer DU. A study on the dependency of the open-circuit voltage on temperature and actual aging state of lithium-ion batteries. J Power Sources 2017;347:1–13. 2017/04/15/.

[13] Waag W, Sauer DU. Adaptive estimation of the electromotive force of the lithium-ion battery after current interruption for an accurate state-of-charge and capacity determination. Appl Energy 2013;111:416–27. 2013/11/01/.

[14] Petzl M, Danzer MA. Advancements in OCV measurement and analysis for lithium-ion batteries. IEEE Trans Energy Convers 2013;28:675–81.

[15] Wei Z, Tseng KJ, Wai N, Lim TM, Skyllas-Kazacos M. Adaptive estimation of state of charge and capacity with online identified battery model for vanadium redox flow battery. J Power Sources 2016;332:389–98. 2016/11/15/.

[16] He H, Xiong R, Guo H. Online estimation of model parameters and state-of-charge of LiFePO4 batteries in electric vehicles. Appl Energy 2012;89:413–20. 2012/01/01/.

[17] Lin C, Yu Q, Xiong R, Wang LY. A study on the impact of open circuit voltage tests on state of charge estimation for lithium-ion batteries. Appl Energy 2017;205:892–902. 2017/11/01/.

[18] Chiang Y-H, Sean W-Y, Ke J-C. Online estimation of internal resistance and open-circuit voltage of lithium-ion batteries in electric vehicles. J Power Sources 2011;196:3921–32. 2011/04/15/.

[19] Hu X, Li S, Peng H. A comparative study of equivalent circuit models for Li-ion batteries. J Power Sources 2012;198:359–67. 2012/01/15/.

[20] Gao W, Zou Y, Sun F, Hu X, Yu Y, Feng S. Data pieces-based parameter identification for lithium-ion battery. J Power Sources 2016;328:174–84. 2016/10/01/.

[21] Yang J, Xia B, Shang Y, Huang W, Mi CC. Adaptive state-of-charge estimation based on a split battery model for electric vehicle applications. In: IEEE Transactions on Vehicular Technology, vol. PP; 2017. p. 1–1.

[22] Plett GL. Extended Kalman filtering for battery management systems of LiPB-based HEV battery packs: Part 2. Modeling and identification. J Power Sources 2004;134:262–76. 2004/08/12/.

[23] Dai H, Wei X, Sun Z, Wang J, Gu W. Online cell SOC estimation of Li-ion battery packs using a dual time-scale Kalman filtering for EV applications. Appl Energy 2012;95:227–37. 2012/07/01/.

[24] Zheng F, Xing Y, Jiang J, Sun B, Kim J, Pecht M. Influence of different open circuit voltage tests on state of charge online estimation for lithium-ion batteries. Appl Energy 2016;183:513–25. 2016/12/01/.

[25] Newman and Srinivasan. Existence of path-dependence in the LiFePO4 electrode. Electrochem Solid-State Lett 2006;9:A110–4.

[26] Antaloae C, Marco J, Assadian F. A novel method for the parameterization of a li-ion cell model for EV/HEV control applications. IEEE Trans Veh Technol 2012;61:3881–92.

[27] Huria T, Ludovici G, Lutzemberger G. State of charge estimation of high power lithium iron phosphate cells. J Power Sources 2014;249:92–102. 2014/03/01/.

[28] Zhu L, Sun Z, Dai H, Wei X. A novel modeling methodology of open circuit voltage hysteresis for LiFePO4 batteries based on an adaptive discrete Preisach model. Appl Energy 2015;155:91–109. 2015/10/01/.

[29] Barai A, Widanage WD, Marco J, McGordon A, Jennings P. A study of the open circuit voltage characterization technique and hysteresis assessment of lithium-ion cells. J Power Sources 2015;295:99–107. 2015/11/01/.

[30] Arora S, Shen W, Kapoor A. Critical analysis of open circuit voltage and its effect on estimation of irreversible heat for Li-ion pouch cells. J Power Sources 2017;350:117–26. 2017/05/15/.

[31] Do DV, Forgez C, Benkara KEK, Friedrich G. Impedance observer for a li-ion battery using Kalman filter. IEEE Trans Veh Technol 2009;58:3930–7.

[32] Schweighofer B, Wegleiter H, Recheis M, Fulmek P. Fast and accurate battery model applicable for EV and HEV simulation. In: 2012 IEEE International Instrumentation and Measurement Technology Conference Proceedings; 2012. p. 565–70.

[33] Vyroubal P, Kazda T. Equivalent circuit model parameters extraction for lithium ion

batteries using electrochemical impedance spectroscopy. J Storage Mater 2018;15:23–31. 2018/02/01/.
[34] Pei L, Wang T, Lu R, Zhu C. Development of a voltage relaxation model for rapid open-circuit voltage prediction in lithium-ion batteries. J Power Sources 2014;253:412–8. 2014/05/01/.
[35] Mu H, Xiong R, Zheng H, Chang Y, Chen Z. A novel fractional order model based state-of-charge estimation method for lithium-ion battery. Appl Energy 2017;207:384–93. 2017/12/01/.
[36] Fleischer C, Waag W, Heyn H-M, Sauer DU. On-line adaptive battery impedance parameter and state estimation considering physical principles in reduced order equivalent circuit battery models: Part 1. Requirements, critical review of methods and modeling. J Power Sources 2014;260:276–91. 2014/08/15/.
[37] Hentunen A, Lehmuspelto T, Suomela J. Time-domain parameter extraction method for thévenin-equivalent circuit battery models. IEEE Trans Energy Convers 2014;29:558–66.
[38] Jossen A. Fundamentals of battery dynamics. J Power Sources 2006;154:530–8. 2006/03/21/.
[39] Kroeze RC, Krein PT. Electrical battery model for use in dynamic electric vehicle simulations. In: 2008 IEEE Power Electronics Specialists Conference; 2008. p. 1336–42.
[40] Andre D, Meiler M, Steiner K, Walz H, Soczka-Guth T, Sauer DU. Characterization of high-power lithium-ion batteries by electrochemical impedance spectroscopy. II: Modelling. J Power Sources 2011;196:5349–56. 2011/06/15/.
[41] Hentunen A. Electrical and thermal characterization of large lithium-ion batteries for non-road mobile machinery applications; 2016.
[42] Diao W, Xue N, Bhattacharjee V, Jiang J, Karabasoglu O, Pecht M. Active battery cell equalization based on residual available energy maximization. Appl Energy 2018;210:690–8. 2018/01/15/.
[43] Yang J, Xia B, Shang Y, Huang W, Mi C. Improved battery parameter estimation method considering operating scenarios for HEV/EV applications. Energies 2016;10:5.
[44] Kang J, Yan F, Zhang P, Du C. Comparison of comprehensive properties of Ni-MH (nickel-metal hydride) and Li-ion (lithium-ion) batteries in terms of energy efficiency. Energy 2014;70:618–25. 2014/06/01/.
[45] Büngeler J, Cattaneo E, Riegel B, Sauer DU. Advantages in energy efficiency of flooded lead-acid batteries when using partial state of charge operation. J Power Sources 2018;375:53–8. 2018/01/31/.
[46] Zhang Y, Song W, Feng Z. An energy efficiency evaluation research based on heat generation behavior of lithium-ion battery. J Electrochem Soc 2013;160:A1927–30.
[47] Zhu WH, Zhu Y, Davis Z, Tatarchuk BJ. Energy efficiency and capacity retention of Ni–MH batteries for storage applications. Appl Energy 2013;106:307–13. 2013/06/01/.